Inelastic seismic analysis of RC bridge piers including flexure-shear-axial interaction

Do Hyung Lee[†]

*Department of Civil and Geotechnical Engineering, Paichai University, 439-6 Doma 2 dong,
Seo-ku, Daejeon, Korea*

Amr S. Elnashai[‡]

*Structural Engineering, 2129e CEE Department, University of Illinois at Urbana-Champaign,
205 North Mathews Avenue, Urbana, IL 61801-2397, USA*

Abstract. The effect of shear coupled with axial force variation on the inelastic seismic behaviour of reinforced concrete bridge piers is investigated in this paper. For this purpose, a hysteretic axial-shear interaction model was developed and implemented in a nonlinear finite element analysis program. Thus, flexure-shear-axial interaction is simulated under variable amplitude reversed actions. Comparative studies for shear-dominated reinforced concrete columns indicated that a conventional FE model based on flexure-axial interaction only gave wholly inadequate results and was therefore incapable of predicting the behaviour of such members. Analysis of a reinforced concrete bridge damaged during the Northridge (California 1994) earthquake demonstrated the importance of shear modelling. The contribution of shear deformation to total displacement was considerable, leading to increased ductility demand. Moreover, the effect of shear with axial force variation can significantly affect strength, stiffness and energy dissipation capacity of reinforced concrete members. It is concluded that flexure-shear-axial interaction should be taken into account in assessing the behaviour of reinforced concrete bridge columns, especially in the presence of high vertical ground motion.

Key words: reinforced concrete; bridges; columns; hysteretic response; shear deformation; axial force variation

1. Introduction

Many reinforced concrete piers or columns of highway bridge structures suffered severe diagonal shear failure during recent earthquakes (e.g., the 1994 Northridge earthquake, USA; Priestley *et al.* 1994, Broderick *et al.* 1994, and the 1995 Hyogoken-Nanbu earthquake, Japan; Seible *et al.* 1995, Elnashai *et al.* 1995). Such severe collapse demonstrated that these members did not have sufficient shear strength and ductility to resist the demand imposed by ground motions. Therefore, an accurate estimation of shear strength and ductility is necessary alongside other action effects, namely flexural and axial.

---

† Lecturer
‡ Professor

Whereas extensive research has been conducted on the determination of shear strength (Ang *et al.* 1989, Preistley *et al.* 1994) and shear deformation (Vecchio and Collins 1986, Hsu 1988) of reinforced concrete columns under constant axial force, very few studies are available on the response of reinforced concrete columns under varying axial force. Studies by Abrams (1987) and Saadeghvaziri and Foutch (1990, 1991) were among those very few studies that took into account the axial force variation. However, these studies were limited with regard to the behaviour of flexure-axial interaction for reinforced concrete columns.

Inelastic deformations generated during seismic response are not limited to flexural deformation. Saatcioglu and Ozcebe (1989) conducted reinforced concrete column tests to study these interactive response issues. The study indicated that inelastic shear deformation can significantly affect total deformation in local areas. In addition, a larger shear capacity compared to that corresponding to flexural capacity does not necessarily ensure elastic shear behaviour. It is therefore important to develop a simple and realistic analytic model that is capable of predicting the behaviour of reinforced concrete columns under flexure-shear-axial interaction.

In view of the above, a hysteretic axial-shear interaction model was developed, and implemented in a finite element program ADAPTIC (1989) that was based on flexure-axial interaction. Consequently, flexure-shear-axial interaction was simulated in the framework of a point hinge modelling approach. Since very few reinforced concrete column tests subjected to continuously varying axial force are available, verification of the model was performed by comparison with experimental results under constant axial force which varied from one test to another. The axial effect model is therefore intuitive with regard to axial force variation during the transverse response regime. Subsequently, validation of the model was resumed in terms of inelastic response analysis of a reinforced concrete bridge, which was severely damaged by the Northridge earthquake.

2. Model description

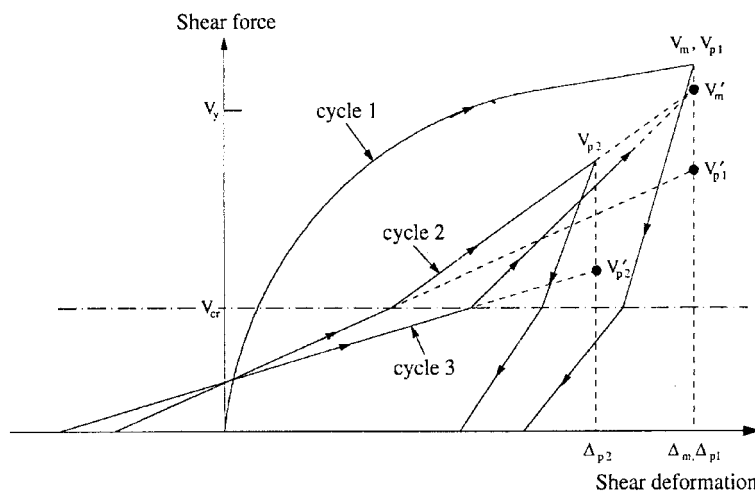To describe the inelastic cyclic response of the hysteretic shear behaviour under axial force

Fig. 1 Sample segments of the reloading branches (Ozcebe and Saatcioglu 1989)

variation, the model proposed by Ozcebe and Saatcioglu (1989) was adopted for investigating loading and unloading (total and partial). Although the model showed good agreement with experiments, direct use of the model in the inelastic time-history analysis was still uncertain since most expressions derived were based on limited experimental data under constant axial force. Hence, further developments were undertaken with respect to the evaluation of reloading stiffness values. In the model, two reference points were used to define the branches below and above the cracking load. The graphical representation of these points and sample reloading branches is shown in fig. 1.

   The co-ordinates of the two reference points are given by,

$$V_p{'}=V_p e^{\alpha\left(\frac{\Delta_p}{\Delta_y}\right)} \tag{1}$$

$$\alpha=0.82\left(\frac{N}{N_o}\right)-0.14 < 0.0 \tag{2}$$

$$V_m{'}=V_m e^{[\beta n + \gamma(\Delta_m/\Delta_y)]} \tag{3}$$

$$\beta=-0.014\sqrt{\frac{\Delta_m}{\Delta_y}} \tag{4}$$

$$\gamma=-0.010\sqrt{n} \tag{5}$$

where Δ_p is the previous peak displacement, Δ_y is the yield displacement, Δ_m is the maximum displacement, $V_p{'}$ is the shear force aimed at the previous peak displacement defining the reloading stiffness below the cracking load, V_p is the previous peak shear force, $V_m{'}$ is the shear force at the maximum displacement defining the reloading stiffness above the cracking load, V_m is the shear force on the primary curve corresponding to maximum displacement, n is a counter and assigned in each direction of loading, N is an applied axial force and N_o is nominal axial compressive capacity based on ACI 318-83 (1983).

   As illustrated in Eqs. (1) and (2), the reloading stiffness below the cracking load is a function of not only axial force but also shear displacement ductility. Since Eq. (2) was derived from two levels of axial compressive load (zero axial load and 11% of axial compressive capacity based on ACI 318-83 (1983) were used in the experiment), a relationship should be defined for other levels of axial force. Linear interpolation was employed hence Eq. (2) can be replaced by,

$$\alpha=0.055249\left(\frac{N}{N_o}\right)-0.055251 < 0.0 \tag{6}$$

On the other hand, few experimental data is available with regard to reinforced concrete columns subjected to tensile axial force. Maruyama *et al.* (1984) conducted reinforced concrete column tests with tensile axial force. The study indicated that shear strength degradation was minor at lower levels of deformation and the reverse was true. In the present study, reloading stiffness was assumed to follow a straight line toward the previous peak point in the direction of loading when tensile axial force was applied. The assumptions given above were supported by the good agreement obtained between analyses and experiment. The detailed description of the above is given in Lee (1999).

The envelope curve for the hysteretic relationship was derived from the Modified Compression Field Theory (1986) (hereafter referred to as MCFT), which provides force-displacement relationships under monotonic loading. The theory was widely used for the analysis of reinforced concrete members and gave good correlation (Vecchio and Collins 1988, Vecchio and Emara 1992). The MCFT employed average stress-average strain relationships in a cracked reinforced concrete element, satisfying compatibility and equilibrium conditions. For the reinforcement, a bilinear stress-strain relationship is used. Thus,

$$f_{ls} = E_{ls}\varepsilon_l \le f_{ly} \tag{7}$$

$$f_{ts} = E_{ts}\varepsilon_t \le f_{ty} \tag{8}$$

where f_{ls} is the longitudinal reinforcement stress, E_{ls} is Young's modulus of longitudinal reinforcement, ε_l is the longitudinal strain, f_{ly} is the yield stress of longitudinal reinforcement, while subscript t in Eq. (8) denotes the parameters in the transverse direction.

For cracked concrete in compression, the average principal compressive stress, f_{c2} is given by,

$$f_{c2} = f_{c2\max}\left[2\left(\frac{\varepsilon_2}{\varepsilon_{co}}\right) - \left(\frac{\varepsilon_2}{\varepsilon_{co}}\right)^2\right] \tag{9}$$

$$\frac{f_{c2\max}}{f_{co}'} = \frac{1}{0.8 - 0.34\varepsilon_1/\varepsilon_{co}} \le 1.0 \tag{10}$$

where $f_{c2\max}$ is the maximum compressive stress of concrete, ε_1 and ε_2 are the principal tensile and compressive strains, respectively and ε_{co} is the strain at peak stress of unconfined concrete, f_{co}'.

For concrete in tension, the average principal tensile stress, f_{c1} prior to cracking is given below,

$$f_{c1} = E_c\varepsilon_1 \tag{11}$$

where $E_c (=2f_{co}'/\varepsilon_{co})$ denotes the initial elastic modulus of concrete.

The average principal tensile stress after cracking is given by,

$$f_{c1} = \frac{f_{cr}}{1 + \sqrt{200\varepsilon_1}} \tag{12}$$

where $f_{cr}(=0.33\sqrt{f_{co}'})$ represents the diagonal cracking stress of concrete.

However, the stress-strain relationship for concrete in compression adopted in Vecchio and Collins (1986) does not simulate effective confinement of the core concrete confined with circular and rectangular hoops. Therefore, a modified stress-strain relationship for concrete in compression with confinement effect was derived. Amongst the concrete models for constant confinement, the model of Mander *et al.* (1988) was appropriate in terms of a balance between accuracy and applicability to various section types. Accordingly, it was adopted in this study. Hence, the principal compressive stress, f_{c2} in Eq. (9) can be replaced by,

$$f_{c2} = v_1\left[\frac{f_{cc}' \, xr}{r - 1 + x^r}\right] \tag{13}$$

$$x = \frac{\varepsilon_c}{\varepsilon_{cc}} \tag{14}$$

$$\varepsilon_{cc} = \varepsilon_{co}\left[1 + 5\left(\frac{f'_{cc}}{f'_{co}} - 1\right)\right] \tag{15}$$

$$r = \frac{E_c}{E_c - E_{sec}} \tag{16}$$

$$E_c = 5000\sqrt{f'_{co}} \tag{17}$$

$$E_{sec} = \frac{f'_{cc}}{\varepsilon_{cc}} \tag{18}$$

where E_{sec} is the secant modulus of elasticity of concrete, ε_{cc} is the strain corresponding peak stress of confined concrete, f'_{cc} and v_1 represents the effectiveness factor given in Eq. (10).

Strain hardening of reinforcement was also taken into account in constitutive relationships. A full description of the analytical procedures is given elsewhere (Lee 1999, Lee and Elnashai 2001).

Based on the new formulations given above, axial-shear interaction characterisation was developed. The basic concept in including the effect of varying axial forces is that the stiffness in the current time step is calculated by introducing appropriate shifts corresponding to the current level of axial force between series of envelope curves derived for constant levels of axial force. This is an equivalent step-wise linear approach. These transitions represent either hardening (increase in stiffness) or softening (decrease in stiffness) of the member due to variation of axial force. Cracking, yielding and ultimate levels are also shifted in accordance with the axial force variation. An overview of the development is given in Elnashai *et al.* (1999) and the graphical representation of the shear stiffness transition due to varying axial forces is illustrated in Fig. 2.

The hysteretic axial-shear interaction model was implemented in a finite element analysis program ADAPTIC (Izzuddin and Elnashai 1989), which has been developed at Imperial College over the past twelve years. The program has been developed for the inelastic nonlinear behaviour of 2-D and 3-D structures. Static, dynamic and eigenvalue solutions are available in the program and have been
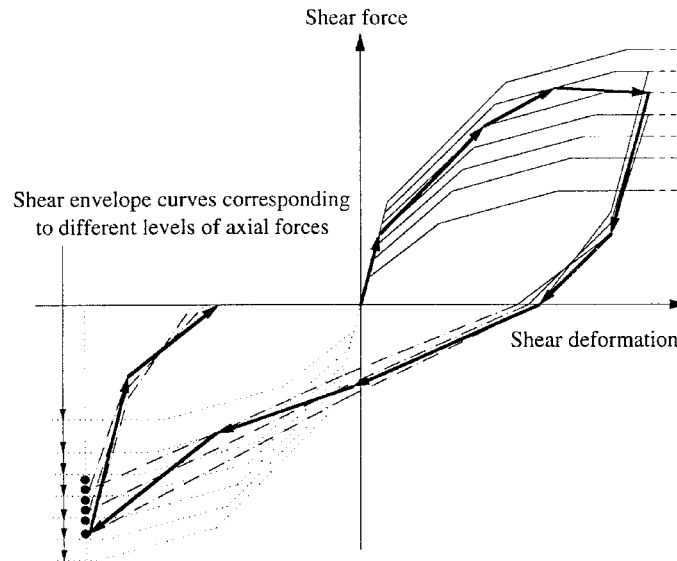

Fig. 2 Shear stiffness transition due to axial force variation

thoroughly tested and validated (Madas and Elnashai 1992, Martinez-Rueda and Elnashai 1997 amongst many others).

The new element takes into account the calculation of force for a given displacement as well as the current level of axial force. Also included is updating of the stiffness matrix at each iteration. In order to ensure continuity when convergence to equilibrium is achieved, storing and updating of the values of force and displacement corresponding to the previous and current displacement increment are necessary. In so doing, the precise location of the branches can be traced. The envelope curves are pre-specified for several different levels of constant axial force. The envelope curve corresponding to an axial force between these pre-specified levels is established by interpolation within the new element. This enables the selection of the axial force range of interest for each structure. A complete description of the implementation is given in Lee (1999).

3. Verification

In order to verify the implementation of the new formulation, the analytical results obtained with ADAPTIC (Izzuddin and Elnashai 1989) incorporating the new element were compared with experimental results from the literature. Comparison was conducted for reinforced concrete columns subjected to constant axial force due to the absence of shear-dominated experimental response observations with continuously varying axial force. Subsequently, earthquake damage observations were employed to investigate the sensitivity and general response characteristics of the axial-shear hysteretic model under dynamic loading conditions in the following section.

An experimental programme described by Maruyama *et al.* (1984) was studied. The test specimen was a short square column the response of which was dominated by shear. A total of 18 specimens were tested including 10 without axial load and 8 with various axial load levels. Fig. 3 shows the test specimen and the cross-section representing a 2/3-scale model of a 450 mm reinforced concrete
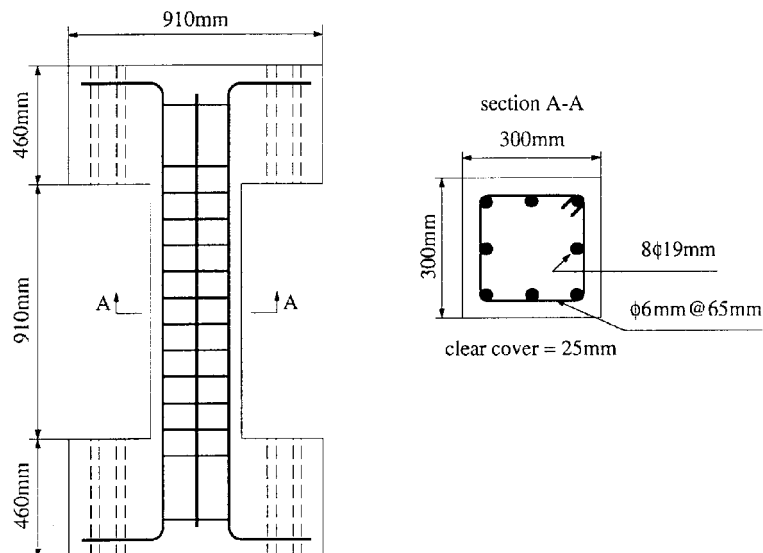

Fig. 3 Dimensions and cross-section details of test specimen (Maruyama *et al.* 1984)

Table 1 Applied axial force and material properties (Maruyama *et al.* 1984)

Specimen	Concrete strength (MPa)	Axial force (kN)	Longitudinal reinforcement		Transverse reinforcement
			Ratio	Yield strength (MPa)	Yield strength (MPa)
O-U	34.5	0.0	0.0252	374	466
120C-U	30.4	528	0.0252	450	466
100T-U	38.6	-440[*]	0.0252	374	466

[*]–ve indicates tensile axial force.

column. A 65 mm spacing of transverse reinforcement corresponding to the maximum spacing specified in ACI 318-71 (1971) was used to ensure that shear behaviour is dominant. The column height-to-depth ratio was 3.0. Three test specimens were selected for comparative studies, O-U, 120C-U and 100T-U subjected to zero, compressive and tensile axial force, respectively. The material properties of the specimens are given in table 1.

The test specimens were modelled using two approaches: (1) a FE model consisting of the conventional cubic inelastic elements and (2) an assembly of cubic inelastic elements and a point hinge element representing the new interactive element described above at the member base. While the former simulates flexure-axial response, the latter represents flexure-shear-axial interaction behaviour.

Figs. 4(a), (b) and (c) depict comparisons between experimental results and analyses with and without shear representation for specimens O-U, 120C-U and 100T-U, respectively. As observed, the hysteretic response of test results shows a significant pinching and, in general, the analyses with shear exhibit good correlation with experimental measurements on the overall inelastic behaviour. Both strength and stiffness degradation are estimated with reasonable accuracy. However, comparisons between experimental measurements and analyses without shear show wholly inadequate results where significant difference is observed in both strength and stiffness. This emphasises that use of FE models based on flexure only is inadequate to predict the response of reinforced concrete members of low shear ratios. Table 2 shows the comparison of strength values between experimental measurements and analyses with shear at each ductility level. Since experimental results of specimens 120C-U and 100T-U are available for first-cycle only, comparisons are undertaken with respect to first-cycle only for those specimens. Although the analytical predictions slightly underestimate the strength, a relatively good agreement is observed within a margin of 10%.

Table 2 Strength comparison between experiment and analysis with shear at different ductility levels

Specimen	Cycle	Peak strength corresponding to each cycle (kN)							
		$\mu=1$		$\mu=2$		$\mu=3$		$\mu=4$	
		Exp.	Anal.	Exp.	Anal.	Exp.	Anal.	Exp.	Anal.
O-U	1st cycle	191.7	191.6	252.1	223.0	258.1	211.7	–	–
	3rd cycle	165.4	158.3	218.3	167.0	210.0	153.5	–	–
120C-U	1st cycle	-	-	285.5	280.0	282.1	246.0	–	–
100T-U	1st cycle	123.0	115.0	148.5	130.0	153.6	142.1	158.6	149.0

(a) Specimen O-U
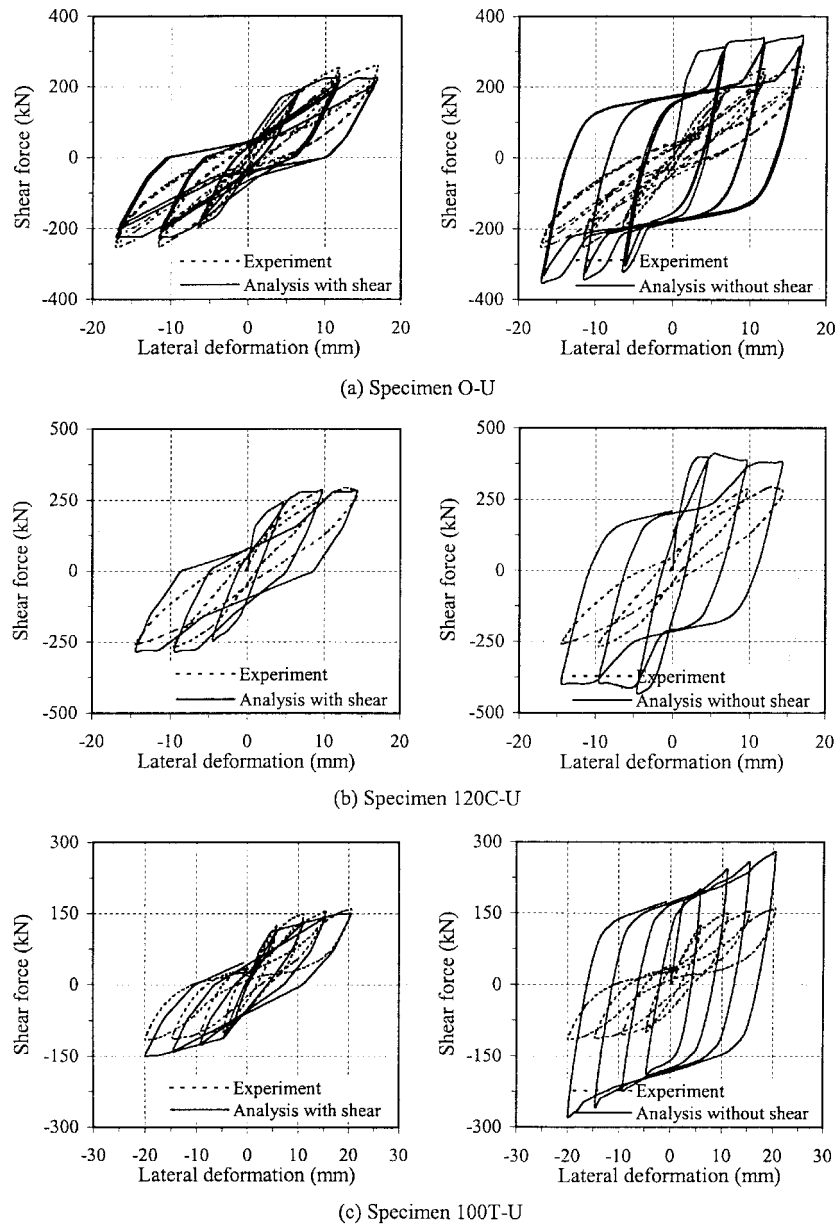
(b) Specimen 120C-U

(c) Specimen 100T-U

Fig. 4 Comparison between experiment and analysis with and without shear

4. Case study: Santa Monica Collector-Distributor 36

The Northridge earthquake of 17 January 1994 caused severe damage to freeway structures, particularly reinforced concrete bridges. The most serious damage occurred in short stiff piers. Detailed description of the earthquake can be found elsewhere (Priestley *et al*. 1994, Broderick *et al.*, 1994 amongst others). Among the bridges damaged by the earthquake is La Cienega-Venice
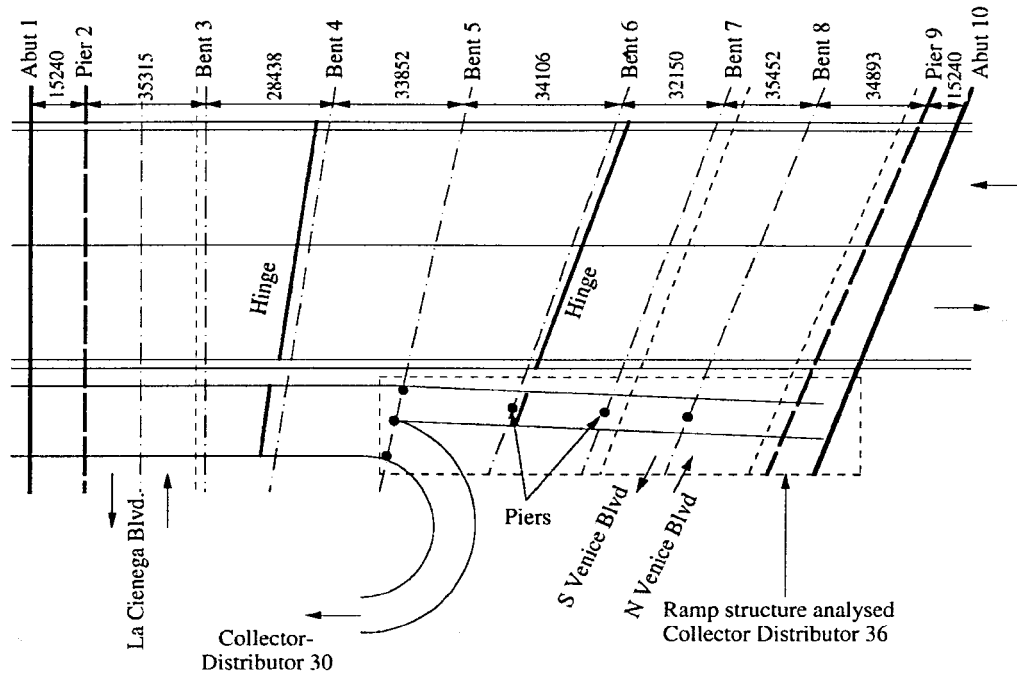
Fig. 5 Plan of I-10 La Cienega-Venice Blvd. undercrossing

Boulevard sector of the I-10 freeway, the subject of the back-analysis presented hereafter. This sector is an independent structure supporting a pair of off-ramps from the eastbound carriageway. These ramps bifurcate between the third and fourth bents when one ramp (Off-ramp 36) follows a circular pattern to connect with La Cienega Boulevard North. The second ramp (Collector-Distributor 36) which is the structure under consideration, continues on a line close to that of the main freeway. The position of the various elements of the undercrossing is shown in Fig. 5.

To investigate the cause of the damage pattern experienced by the ramp structure and to define the most salient features of its behaviour, the ramp structure was subjected to detailed analysis using the new element to compare observed and predicted damage.

5.1 Description of the ramp structure

The deck of the ramp structure consists of a three-celled box girder. From the bifurcation point to the west of bents, the deck is carried over the multi-column bent 5, then over three single column bents 6, 7 and 8, and over the pier wall of bent 9 to the east abutment. In the deck, a movement joint forming a structural hinge is placed approximately 5 m away from bent 6.

The columns of all bents consist of 1219 mm diameter reinforced concrete circular sections. Whereas bents 6, 7 and 8 are single columns, bent 5 comprises three columns, two of which support the ramp structure and one supports the adjacent circular off-ramp. Column longitudinal reinforcement is identical for piers 6, 7 and 8, while less longitudinal reinforcement is employed in the columns of bent 5. Figs. 6(a) and (b) show an idealised cross-section of the deck girder and the two types of column cross-sections, respectively. Bent 9 is supported by a wall the cross-section of
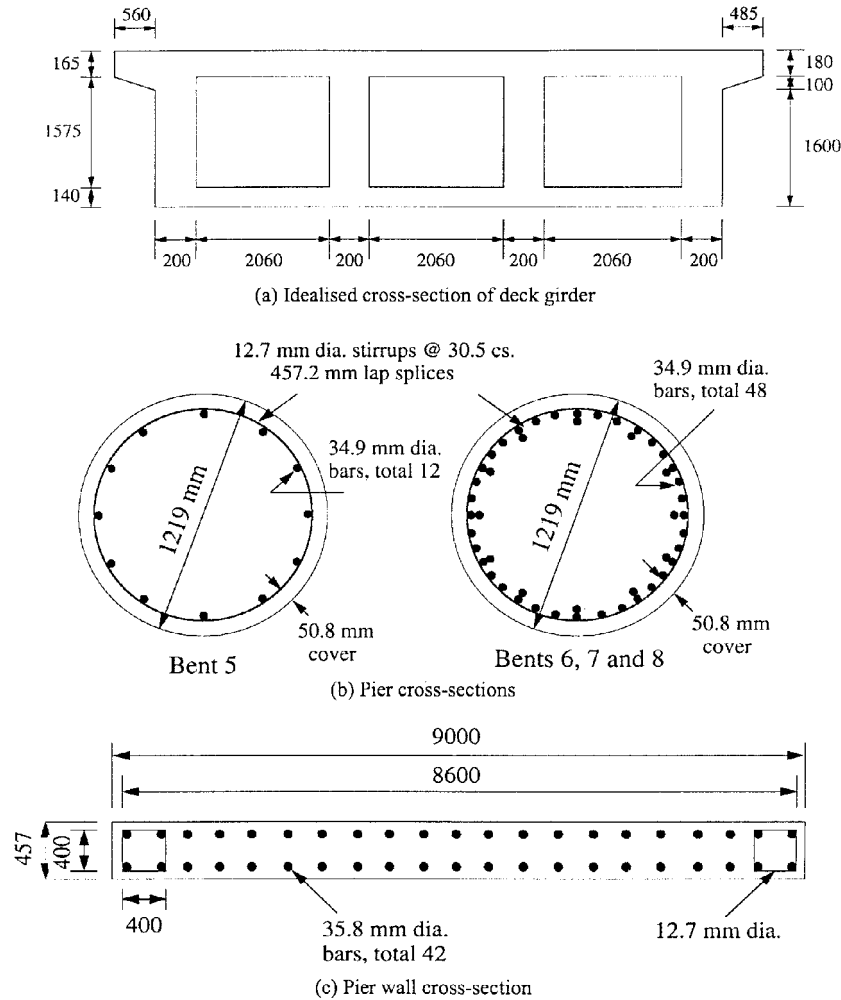
(a) Idealised cross-section of deck girder

12.7 mm dia. stirrups @ 30.5 cs.
457.2 mm lap splices

34.9 mm dia.
bars, total 48

34.9 mm dia.
bars, total 12

1219 mm

1219 mm

50.8 mm
cover

Bent 5

50.8 mm
cover

Bents 6, 7 and 8

(b) Pier cross-sections

9000

8600

457

400

400

35.8 mm dia.
bars, total 42

12.7 mm dia.

(c) Pier wall cross-section

Fig. 6 Cross-sections of deck and piers

which is shown in Fig. 6(c). The longitudinal reinforcement is continuous to the bottom of the footing. The connection between the piers and the deck is also effectively continuous.

5.2 Description of damage

The most damaged column of all was pier 6, which experienced severe cracking. The cover concrete spalled completely over its height and the core concrete disintegrated. Buckling occurred in all of the longitudinal reinforcement and the confining hoops ruptured. Whereas no damage was detected in pier 7, damage to pier 8 was again significant. Severe shear cracking occurred in the lower half of the column. Much spalling occurred at the latter location with some buckling of longitudinal reinforcement. No visible damage was reported in either the ramp deck or abutment. A photograph of damage is shown in Fig. 7.
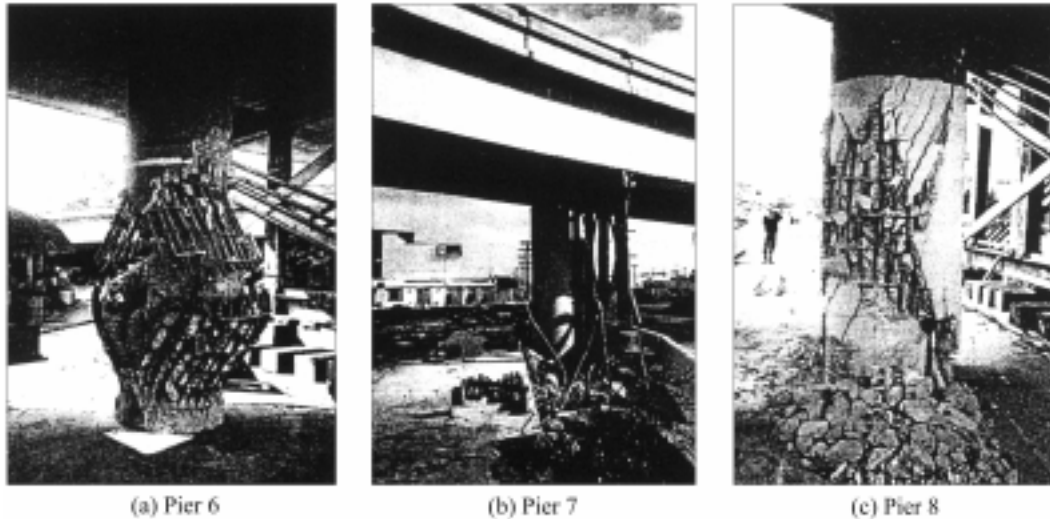
Fig. 7 Damage pattern of piers

5.3 Modelling assumptions

The general layout of the ramp structure is shown in Fig. 8(a). In this model, five cubic inelastic elements were employed in the piers, with shorter elements at the base and top of the piers and longer elements towards the centre. Such an arrangement allowed potential plastic hinge zones to be accurately captured.

The deck was modelled using one quartic elastic element per span. No live loads were imposed on the bridge since the Northridge earthquake occurred at 4:31 am. Gravity loads were assessed from the cross-sectional areas of the box-girder and the piers. A nominal allowance was also made for a 100 mm thickness of pavement.

The deck hinge was modelled using a 3-D joint element allowing free rotations in the longitudinal plane of the deck and about the vertical axis. The bridge deck was assumed to be fully restrained at its intersection with bent 5. This reflected the relative dimensions of the ramp on either side of this point, which suggested that a relatively insignificant amount of transverse deformation would occur to the west of bent 5. A moment release was assumed at the east abutment.

To account for the effect of shear, each pier of the ramp structure was modelled by a combination of cubic inelastic elements with a single joint element representing axial-shear interaction at the bottom of the piers. The graphical representation of the structural model with shear, i.e., flexure-shear-axial interaction, is shown in Fig. 8(b).

MCFT was used to define the input parameters of the new element. Each pier was analysed for several levels of constant axial force of 10%, 20% and 30% of compressive axial force capacity, zero axial force, and 10% and 30% of the tensile axial force capacity (both capacity values were calculated according to ACI 318-83, 1983). Since the exceedence of 15% of compressive axial force capacity was not common for reinforced concrete bridge columns (Priestley and Benzoni 1996), the choice of the above axial force range was an upper-bound.
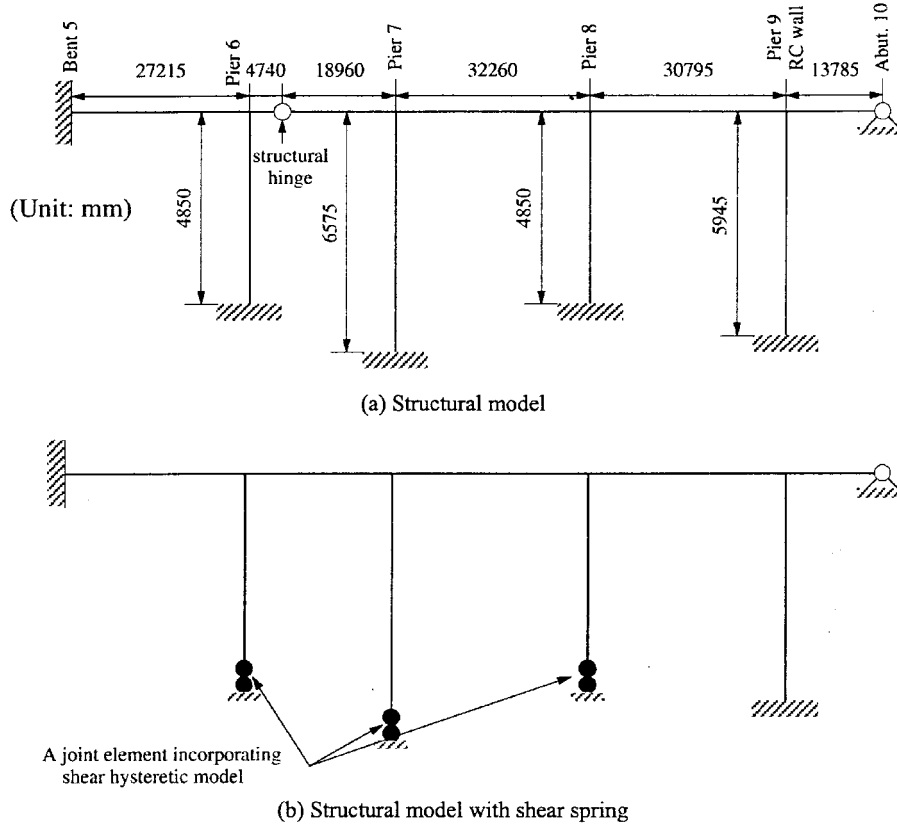
(a) Structural model

(b) Structural model with shear spring

Fig. 8 Analytical models of the ramp structure

5.4 Static analysis

For preliminary evaluation of the column capacities, static analysis of each column was carried out using the MCFT which provided force-displacement relationships. In the static analyses, axial forces corresponding to the gravity loads were applied at the top of each pier. Comparison of shear force-displacement response of piers showed that the response of piers 6 and 8 were nearly identical but slightly higher that for pier 8. This is attributed to larger axial force in pier 8 due to different span length. The response of pier 7 exhibited lower stiffness than that of piers 6 and 8, and experienced greater displacement. This is because of different heights between the piers (piers 6 and 8 are shorter than pier 7). Comparison of the shear force-displacement response of piers is shown in Fig. 9.

Table 3 summarised applied axial force, shear force capacity and yield displacement of the piers. As observed, whereas piers 6 and 8 experienced an identical yield displacement of 32 mm at a curvature of 0.00342/m and 0.00344/m, respectively, the yield displacement experienced by pier 7 was much greater (62 mm corresponding to a curvature of 0.00489/m).

5.5 Dynamic analysis

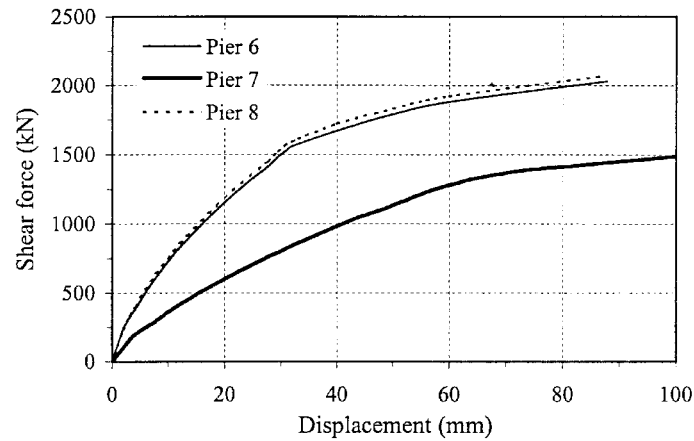The input motions employed in the dynamic analyses were the accelerograms recorded at the City

Fig. 9 Shear force-displacement response of piers

Table 3 Static response parameters

Pier	Axial force (kN)	Shear force (kN)	Yield displacement (mm)
Pier 6	2395	2030	32
Pier 7	2830	1645	62
Pier 8	3180	2065	32

Hall grounds in Santa Monica, approximately 10 km from the location of the La Cienega-Venice undercrossing. This was the closest station to the structure. Peak ground accelerations of the records were 0.883 g, 0.346 g and 0.230 g for transverse, longitudinal and vertical component, respectively. Since the strongest motion occurred at 10 seconds and died gradually after 15 seconds, the first 20 seconds of all components were applied in the dynamic analyses.

Comparison of the displacement time-history response with and without shear subjected to three components was undertaken to investigate the effect of shear on the failure mode of the structure. Fig. 10 shows the transverse displacement response with and without shear for all piers. Whereas response periods are nearly identical, the increase in displacement due to the effect of shear was obvious. In particular, difference in the displacement response with and without shear became significant after 12 seconds at which time the maximum displacements were experienced in all piers. This indicates that piers are subjected to higher displacement demands due to shear (approximately 30% higher), hence more damage is expected to occur.

Maximum displacement experienced by pier 7 did not exceed the yield displacement (62 mm) for both cases (with and without shear), which confirmed that the response of pier 7 remained within elastic range. Whilst maximum displacement without shear for pier 6 (27 mm) did not exceed the yield displacement of 32 mm, that with shear experienced inelastic deformation (35 mm). The same trend was also observed for pier 8. The breakdown of total displacement into its components showed that shear displacement reached a significant level, particularly for piers 6 and 8. The contribution of shear displacement to total displacement was 47% and 44% for piers 6 and 8, respectively. Pier 7 gave a lower value of 25%. The maximum response parameters with regard to displacements and shear forces are summarised in Table 4.
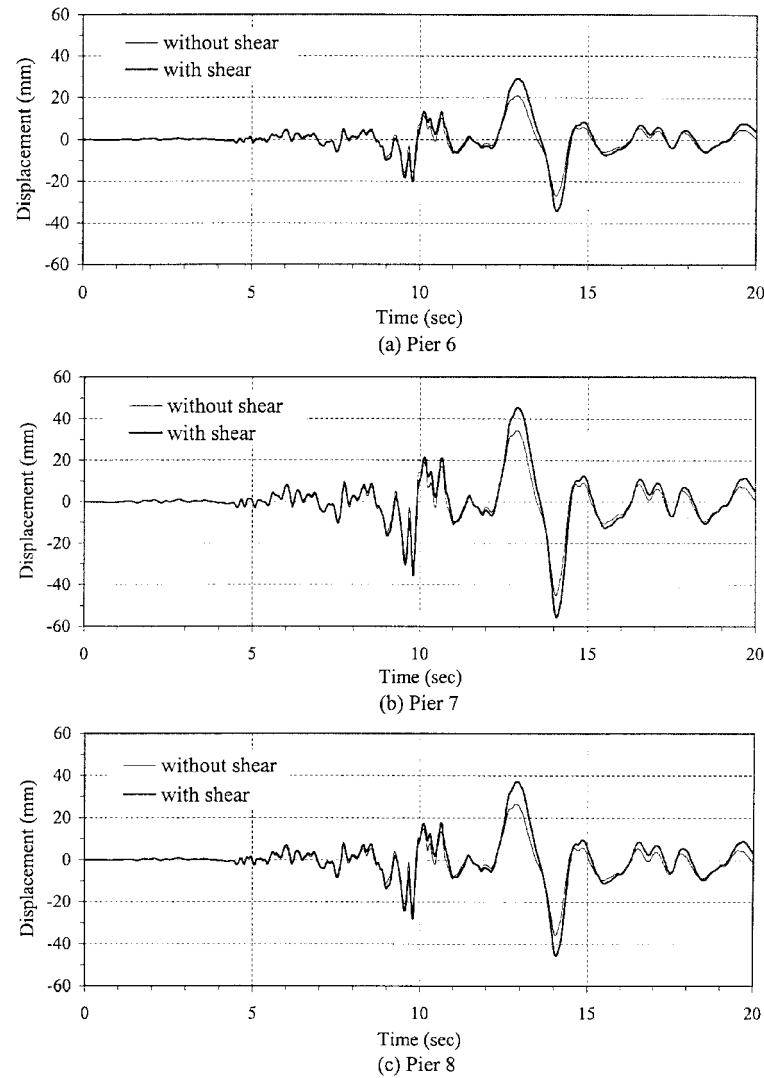
Fig. 10 Transverse displacement response of piers

Table 4 Maximum transverse response parameters

Pier	Flexure-axial interaction		Flexure-shear-axial interaction		
	Displacement (mm)	Shear force (kN)	Total displacement (mm)	Shear force (kN)	Shear displacement (mm)
Pier 6	27.1	2291	35.1	1747	16
Pier 7	45.1	1442	55.7	1510	14
Pier 8	35.8	2654	45.5	2104	20

Shown in Fig. 11 is the transverse shear force response for all piers. Reduction in shear force carrying capacity for the response with shear was pronounced for piers 6 and 8. This indicated that
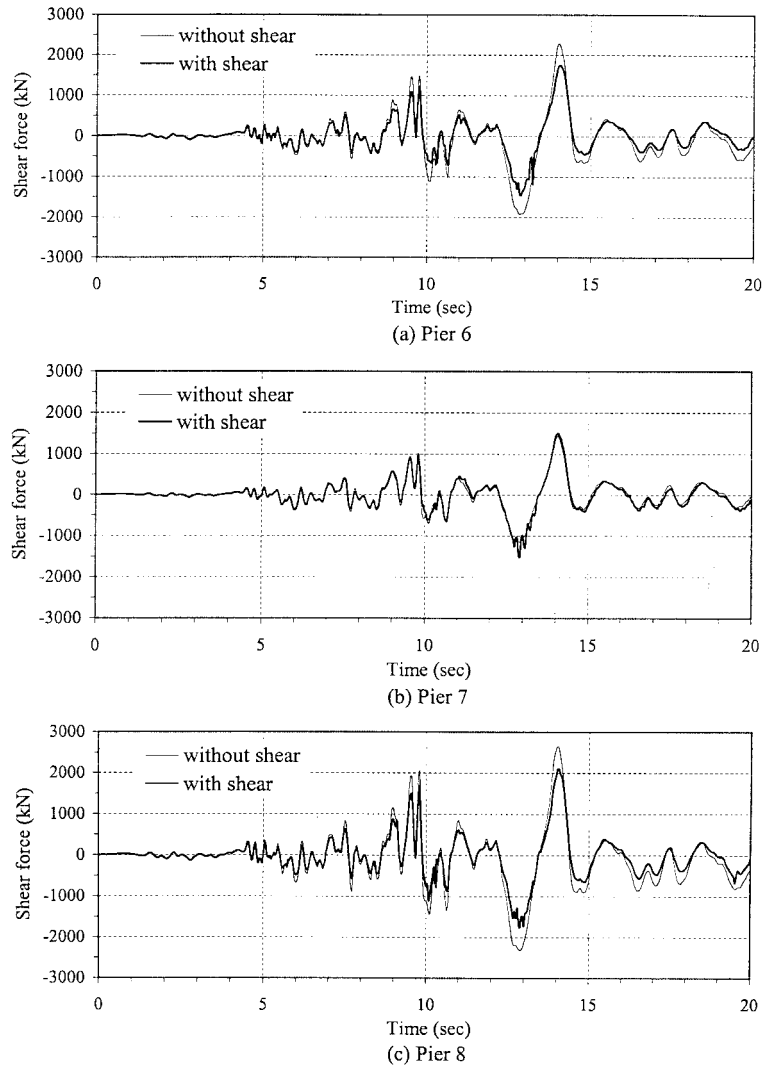
Fig. 11 Transverse shear force response of piers

piers 6 and 8 experienced significant stiffness degradation due to both increase in displacement and decrease in strength. Hence much damage should be expected to occur in the piers. This is supported further by investigation of the hysteresis loops.

Fig. 12 depicts transverse hysteretic response of all piers. The response with shear showed severe stiffness degradation, increased displacement demand and reduced shear force carrying capacity, particularly for piers 6 and 8. In addition, pronounced stiffness and strength fluctuation (even negative stiffness) was also shown in the figure for the response with shear. This negative stiffness is attributed to the axial force variation, coupled with shear. Compressive axial force increases the shear capacity. It is noteworthy that higher axial forces increase the shear capacity, but tend to increase the force demand also, due to period shortening. Therefore, it is possible for shear failure to occur even when the axial force is compressive. On the other hand, tensile axial force decreases
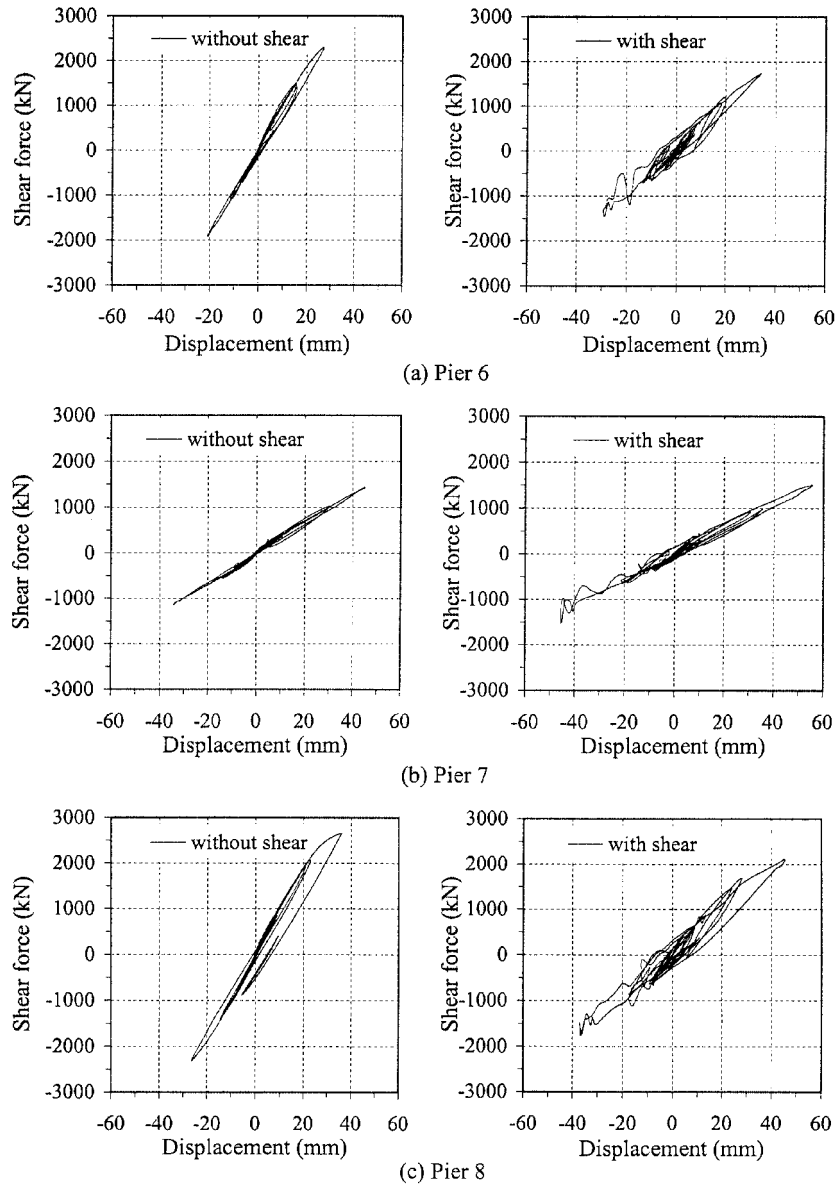
Fig. 12 Transverse hysteretic response of piers

the shear capacity, which may also lead to shear failure. Moreover, the amount of energy absorbed and dissipated by piers can be significantly affected due to axial force variation.

Axial force response of piers is shown in Fig. 13. The response with shear shows significant axial force variation, particularly for piers 6 and 8. This is attributed to the fact that since ductility demand is increased due to shear, corresponding shear force demand is also shifted (either higher or lower depending on governing action through the interaction between flexure and shear). Therefore, higher shear force demand attracts higher compressive axial force and lower shear force demand draws lower compressive axial force (or tensile axial force). This emphasises the importance of the
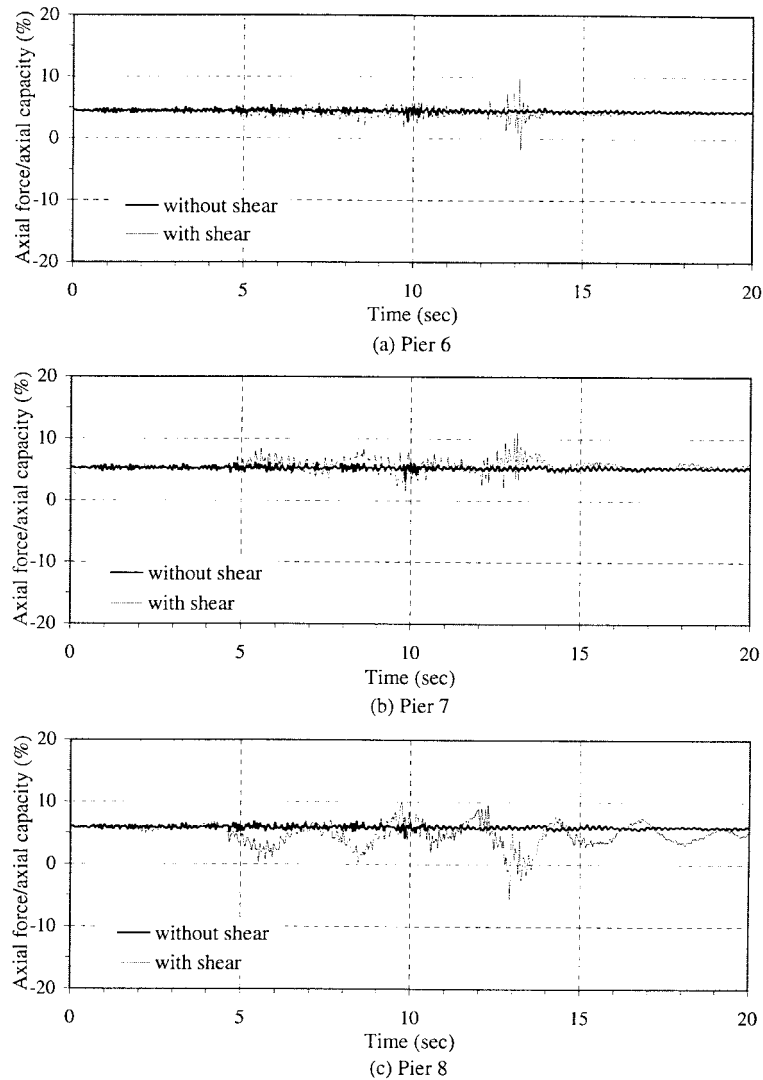
Fig. 13 Axial force response of piers

current development since shear capacity of reinforced concrete columns is affected by the level of axial force. Considering flexure-axial interaction only may lead to both inaccuracy and uncertainty in the shear capacity. It is worthy of mention in Fig. 13 that the response of piers 6 and 8 experiences tensile axial force (-ve indicates tensile axial force) after 12 seconds at which maximum displacements occur in both piers. Therefore, lower shear capacity than expected is likely to occur. This correlates well with the observed damage. Piers 6 and 8 suffered severe shear failure. As mentioned earlier, the response with shear in the piers showed that shear displacement was significant (approximately 50% of the total displacement) and the reduction in shear force carrying capacity was pronounced. Observing the hysteretic response with shear correlated well with the observed damage. The hysteretic response under flexure-shear-axial interaction exhibited severe fluctuation in both strength and stiffness. Also demonstrated was significant stiffness degradation in
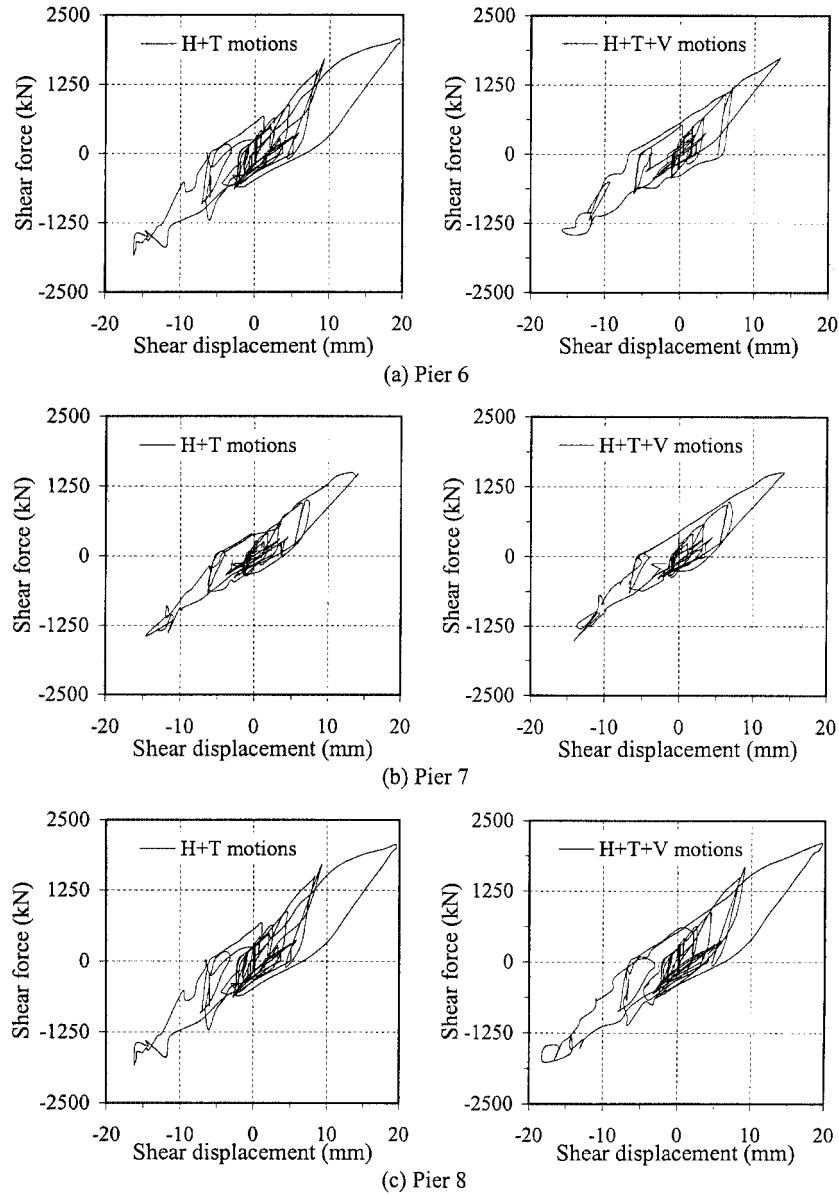
Fig. 14 Transverse hysteretic response with and without vertical ground motion

piers 6 and 8, in comparison with the response of the same piers under flexure-axial interaction. In short, the response under flexure-shear-axial interaction provides better predictions of the observed damage and demonstrates the importance of the current development.

Further investigation of the failure modes was carried out in terms of the hysteretic response with and without vertical ground motion. In Fig. 14 the transverse hysteretic response with and without vertical ground motion is shown. Whereas the response of piers 7 and 8 showed little difference, this was not the case for pier 6. Energy absorption capacity of pier 6 was considerably affected by the presence of the vertical ground motion. This suggested that vertical ground motion affected the

failure mode experienced by pier 6. It also explains the observed damage of pier 6 further, i.e., low energy absorption capacity and sudden drop in shear force carrying capacity due to the combined effect of shear and vertical ground motion (or axial force variation).

6. Conclusions

A hysteretic shear model for axial force variation was developed and implemented in the nonlinear static and dynamic analysis program ADAPTIC, in order to simulate flexure-shear-axial interaction. Verification of the new model was achieved by comparison with shear-dominated reinforced concrete columns subjected to several levels of constant axial force. The comparison showed that conventional flexural models gave wholly unreliable results for such members, while that with the current development provided good correlation in terms of strength, stiffness and energy absorption capacities.

Inelastic seismic analyses were also performed on a reinforced concrete bridge damaged during the Northridge earthquake. The evaluation of displacements indicated that shear displacements can reach significant levels (up to 50% of total displacements), thus increasing the imposed ductility demand by up to 30%. In addition, hysteretic response demonstrated that the effect of shear coupled with axial force variation can significantly affect strength, stiffness and energy dissipation capacity of reinforced concrete members. Pronounced fluctuation in both strength and stiffness was observed in the response using flexure-shear-axial interaction, whilst the response under flexure-axial interaction did not pick such effects. In short, considering flexure-axial interaction only may lead to unrealistic estimation of shear capacity for reinforced concrete columns and thus cause unexpected failure of such members. Another important factor considered was vertical ground motion. Deformation characteristics and energy absorption capacity were demonstrably affected by vertical ground motion. It is therefore recommended that determination of seismic shear capacities of reinforced concrete columns should be based on flexure-shear-axial interaction under horizontal and vertical ground motions, especially in the vicinity of active faults.

References

Abrams, D.P. (1987), "Influence of axial force variations on flexural behavior of reinforced concrete columns", *ACI Structural J.* **84**(3), 246-254.

ACI 318-71 (1971), "Building code requirements for reinforced concrete", American Concrete Institute, Detroit, Michigan, USA.

ACI 318-83 (1983), "Building code requirements for reinforced concrete", American Concrete Institute, Detroit, Michigan, USA.

Ang, B.G., Priestley, M.J.N., and Paulay, T. (1989), "Seismic shear strength of circular reinforced concrete columns", *ACI Structural J.* **86**(1), 45-59.

Broderick, B.M., Elnashai, A.S., Ambraseys, N.N., Barr, J.M., Goodfellow, R.G., and Higazy, E.M. (1994), "The Northridge (California) earthquake of 17 January 1994: observations, strong motion and correlative response analyses", *ESEE research report, No. 94/4*, Imperial College, London.

Elnashai, A.S., Bommer, J.J., Baron, C.I., Lee, D., and Salama, A.I. (1995), "Selected engineering seismology and structural engineering studies of the Hyogo-Ken Nanbu (Great Hanshin) earthquake of 17 January 1995", *ESEE research report, No. 95-2*, Imperial College, London.

Elnashai, A.S., Mwafy, A.M., and Lee, D.H. (1999), "Collapse analysis of RC structures including shear",

Structures Congress of American Society of Civil Engineers, New Orleans, USA.

Hsu, T.T.C. (1988), "Softened truss model theory for shear and torsion", *ACI Structural J.* **85**(6), 624-635.

Izzuddin, B.A., and Elnashai, A.S. (1989), "ADAPTIC A program for static and dynamic analysis of structures by adaptive mesh refinement, user manual", *ESEE research report, No. 89/7*, Imperial College, London.

Lee, D.H. (1999), "Inelastic seismic analysis and behaviour of RC bridges", Ph.D. thesis, Imperial College, London.

Lee, D.H., and Elnashai, A.S. (2001), "Seismic analysis of RC bridge columns with flexure-shear interaction", *J. of Struct. Eng.*, ASCE **127**(5), 546-553.

Madas, P.J., and Elnashai, A.S. (1992), "A new passive confinement model for the analysis of concrete structures subjected to cyclic and transient dynamic loading", *Earthq. Eng. and Struct. Dyn.* **21**, 409-431.

Mander, J.B., Priestley, M.J.N., and Park, R. (1988), "Theoretical stress-strain model for confined concrete", *J. of Struct. Eng.*, ASCE **114**(8), 1804-1826.

Martinez-Rueda, J.E., and Elnashai, A.S. (1997), "Confined concrete model under cyclic loading", *Materials and Structures* **30**, 139-147.

Maruyama, K., Ramirez, H., and Jirsa, J.O. (1984), "Short RC columns under bilateral load histories", *J. of Struct. Eng.*, ASCE **110**(1), 120-137.

Ozcebe, G., and Saatcioglu, M. (1989), "Hysteretic shear model for reinforced concrete members", *J. of Struct. Eng.*, ASCE **115**(1), 132-148.

Priestley, M.J.N., and Benzoni, G. (1996), "Seismic performance of circular columns with low longitudinal reinforced ratios", *ACI Structural J.* **93**(4), 474-485.

Priestley, M.J.N., Seible, F., and Uang, C.M. (1994), "The Northridge earthquake of January 17, 1994: damage analysis of selected freeway bridges", *Structural Systems Research Project, Report No. SSRP-94/06*, University of California, San Diego.

Priestley, M.J.N., Verma, R., and Xiao, Y. (1994), "Seismic shear strength of reinforced concrete columns", *J. of Struct. Eng.*, ASCE **120**(8), 2310-2329.

Saadeghvaziri, M.A., and Foutch, D.A. (1990), "Behavior of RC columns under nonproportionally varying axial load", *J. of Struct. Eng.*, ASCE **116**(7), 1835-1856.

Saadeghvaziri, M.A., and Foutch, D.A. (1991), "Dynamic behaviour of R/C highway bridges under the combined effect of vertical and horizontal earthquake motions", *Earthq. Eng. and Struct. Dyn.* **20**, 535-549.

Saatcioglu, M., and Ozcebe, G. (1989), "Response of reinforced concrete columns to simulated seismic loading", *ACI Structural J.* **86**(1), 3-12.

Seible, F., Priestley, M.J.N., and MacRae, G. (1995), "The Kobe earthquake of January 17, 1995", *Structural Systems Research Project, Report No. SSRP-95/03*, University of California, San Diego.

Vecchio, F.J., and Collins, M.P. (1986), "The modified compression field theory for reinforced concrete elements subjected to shear", *ACI Structural J.* **83**(2), 219-231.

Vecchio, F.J., and Collins, M.P. (1988), "Predicting the response of reinforced concrete beams subjected to shear using modified compression field theory", *ACI Structural J.* **85**(3), 258-268.

Vecchio, F.J., and Emara, M.B. (1992), "Shear deformations in reinforced concrete frames", *ACI Structural J.* **89**(1), 46-56.